WELDING RESEARCH

SUPPLEMENT TO THE WELDING JOURNAL, FEBRUARY, 1985

Sponsored by the American Welding Society and the Welding Research Council

TECHNICAL PAPERS EDITOR: T.P. SCHOONMAKER

Thermal Processes in Covered Electrodes

Melting rate is found to be controlled by electromagnetically induced fluid flow in the electrode tip

BY J. H. WASZINK AND M. J. PIENA

ABSTRACT. The decreasing length and the temperature of the covered electrode core were measured as a function of time during welding. Mild steel basic and rutile-type electrodes were used. The results yielded the rate of heat flow from the anode or cathode surface on the liquid tip, through the liquid metal, to the solid wire.

It was found that this process provides the major part of the heat which causes the metal to melt. The corresponding power was found to be proportional to the electric current, and to increase, in general, with increase in electrode diameter.

A physical model, which ascribes the heat transfer to electromagnetically induced fluid flow, accounts for the dependence on the electric current. Thermal processes in a typical electrode were determined experimentally.

Introduction

This paper reports on an investigation of the physical processes that control the melting rate of covered electrodes used for shielded metal arc (SMA) welding. The major part of previous work concerned with this type of electrode dealt with the influence of the flux and operating conditions on the properties of the weld metal.

Previous work has been surveyed by Boniszewski (Ref. 1). Furthermore, the transfer of metal from the electrode tip has been investigated (Refs. 2-6). Examination of the effect of numerous parameters on the melting rate (Refs. 4,7,8) showed an influence exerted by electrode diameter, composition, covering thickness, and polarity. On the other hand, no treatment has yet been given, to the authors' knowledge, to the melting rate in terms of the heat generation and heat transfer processes occurring in an electrode. The work described here was done in order to identify these processes.

Joule Heating and Some Related Effects

The heat required to melt a consumable electrode is, in general, provided by cathode or anode processes occurring at the surface of the liquid tip, and by Joule heating (Ref. 9). Joule heating causes a gradual increase in the temperature of the metal core and the covering, because the latter is heated by conductive heat flow from the core. The covering at the upper end of the electrode must not melt or decompose before the electrode has been melted back completely. Therefore, the electric current has to be chosen such that the temperature remains below a given maximum usually far below the melting point of the metal.

It follows that only a minor part of the thermal energy required to heat and melt the electrode is provided by Joule heating; the major part must be provided by processes occurring at the liquid tip where the electrode is in contact with the arc plasma. The power generated there is equal to $I V_0$ (Fig. 1), where I is the electric current and V_0 is a constant which, in general, depends on polarity, on the composition of the metal at the tip surface and on the properties of the plasma. A part of this power is lost by radiation and by evaporation of material from the surface. The remainder is absorbed by the liquid metal; this, in turn, gives off a thermal power Φ to the solid metal. This heat flow Φ leads to the heating and subsequent melting of the metal core.

The net power absorbed by the liquid metal is given by $\mu\ c_{pl}\ (\overline{T}_{dr} - T_m)$;* the power balance equation for the liquid tip now reads:

$$I V_0 = \Phi + \mu\ c_{pl}\ (\overline{T}_{dr} - T_{mp}) + \Phi_L \quad (1)$$

where Φ_L is the power loss by radiation

Paper presented at the 65th Annual AWS Convention held in Dallas, Texas, during April 8-13, 1984.

J. H. WASZINK and M. J. PIENA are with Philips Research Laboratories, Eindhoven, The Netherlands.

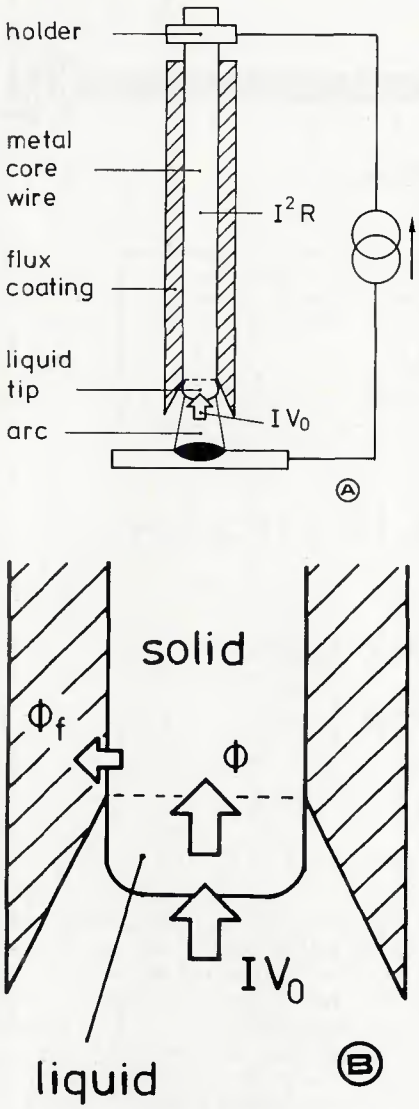

Fig. 1—Illustration of thermal processes in covered electrodes: A—electrode; B—detail of liquid tip

Table 1—Definitions of Symbols[a]

a	Thermal diffusivity, $\lambda/\rho\ c_p$, $m^2\ s^{-1}$
c_p	Specific heat capacity, J kg^{-1} $(°C)^{-1}$ (= 0.239×10^{-3} Btu lb^{-1} $(°F)^{-1}$)
d_f	Outer diameter of coating, m (= 39.37 in.)
d_w	Electrode diameter, m
H	Heat content (see text), J kg^{-1} (= 0.431 Btu lb^{-1})
H_{mp}	Melting energy (see text), J kg^{-1}
I	Electric current, A
L_e	Length of electrode, m
j	Current density in solid wire, A m^{-2}
S_w	Cross-sectional area of wire, m^2
T	Temperature, °C (T (°F) = 1.8 × T (°C) + 32)
T_0	Room temperature, °C
$\overline{T}_{dr}$	Average temperature of pendent drop, °C
T_{mp}	Melting point, °C
T_w	Temperature in main body of solid wire, °C
t	Time, s
u_e	Linear velocity of electrode, m s^{-1} (= 2362 in. min^{-1})
V_0	Anode (cathode) power per ampere, V
z	Axial coordinate, m
λ	Thermal conductivity, W m^{-1} $(°C)^{-1}$ (= 0.803×10^{-3} Btu min^{-1} $in.^{-1}$ $(°F)^{-1}$)
μ	Wire mass melted per unit time, kg s^{-1} (= 132 lb min^{-1})
ν	Kinematic viscosity, $m^2\ s^{-1}$
ρ	Mass density, kg m^{-3} (= 3.61×10^5 lb $in.^{-3}$)
ρ_R	Resistivity, Ω m
Φ	Heat flow rate through tip, W (= 3.41 Btu h^{-1})
Φ_f	Rate of heat flow to flux near fusion boundary, W
Φ_w	Net rate of heat flow to wire, W
Subscripts:	
dr	Pendent drop
e	Electrode, electron
f	Flux
l	Liquid metal
mp	Melting point
w	Solid wire material

(a) Only symbols which are used in more than one portion of the paper are given. Symbols used only once are defined in text.

and evaporation from the tip surface.

Figure 2 shows the distribution of the temperature of the solid metal core along the electrode. The profile is flat along practically the whole length. However, T decreases towards the holder and increases rapidly towards the melting front, so that axial heat flow will occur only in these transition regions. The temperature in the flat portion, T_w, increases with time.

Simple estimates based on the literature (Refs. 10, 11) showed that the transition region adjacent to the holder has a length of a few cm and the transition region near the melting front, Δz, has a length of about 1 mm (0.04 in.) In the latter region, the core is much hotter than the surrounding flux. As a result, there is an appreciable radial heat flow from the core into the flux in this narrow region. The corresponding thermal power will be denoted by Φ_f. The thermal power Φ is used to heat up the metal from T_w to T_{mp}, to melt it, and to provide the power Φ_f.

Experiments that were conducted consisted of measurements of the electrode length and T_w as a function of time in wide ranges of I and d_w. The following covered electrodes were used (Table 2):

1. A thickly coated rutile electrode (R1).
2. A thinly coated rutile electrode (R2).
3. A high-recovery rutile electrode (R3).
4. A normal low-hydrogen electrode (B1).
5. A low-hydrogen electrode having a coating which consisted of two layers of different chemical composition (B2).

Measurements with bare electrodes were also made. The material was mild steel (0.06-0.10% C, 0.45-0.60% Mn); its composition was the same for all the electrodes used.

Arc length was always chosen such that no short circuits occurred between electrode tip and weld pool. This was done in order to keep the system as simple as possible, the aim of this work being the investigation of physical processes. Also measured were the thermal properties of the flux material. Furthermore, high-speed x-ray films of the electrode tip were made in order to verify whether a sizeable heat transfer from the pendent drop to the conical cup in the surrounding covering is likely to occur.

Experiments

All experiments were carried out in the flat welding position, at direct current, with a current-controlled power source (ripple less than 1A). The arc length was chosen such that the electrode tip did not touch the weld pool. In the first series of experiments, a number of electrodes from the same batch was welded at fixed polarity and current, while the welding time was varied. The length of the electrodes was measured before and after welding. This experiment yielded L_e at a number of time points for given I and d_w—Fig. 3.

An automatic electrode feeder was used in the second series of experiments. This device fed the electrode at a velocity

**Definitions of the symbols used throughout the paper are given in Table 1.*

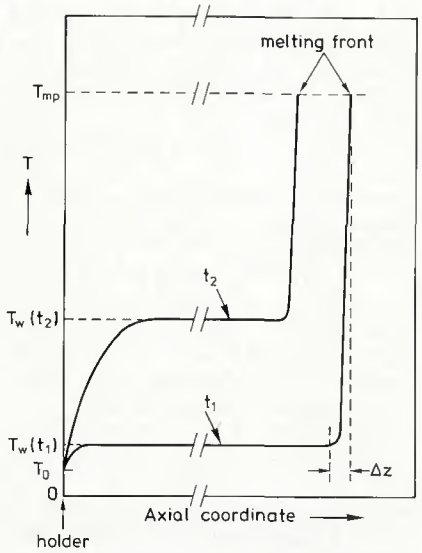

Fig. 2 — Temperature distribution in core along axis of electrode at different times — $t_2 > t_1$

such that the arc length remained constant. This velocity was measured by a tachogenerator, and the data were integrated by a data processor. The curve of L_e vs. t was thus obtained with a single electrode. As a check, the length was measured before and after welding.

The temperature T_w (Fig. 2) was derived from the (strongly temperature-dependent) resistivity, ρ_R, of the steel, which was measured as a function of time. For this purpose, an electrode from the same batch was mounted between two contacts, and two probes were placed on the metal core through small holes in the covering. The same current used in the welding experiment was applied, and the voltage between the probes recorded as a function of time. The probes were always located in the flat part of the temperature profile (see Fig. 2).

The curve of resistivity vs. temperature was obtained in the following way. A thin bare electrode (d_w = 1.6 mm = 0.063 in.) was heated quickly by a current pulse (460 A, 0.2 s), while I and the voltage V, across it, were measured as a function of time. The energy suppplied to the electrode in the interval between t = o and $t = \tau$ is given by:

$$E(\tau) = \int_o^\tau I(t)V(t)dt.$$

Heat losses to the surroundings are negligible in this short time. Consequently,

$$H\{T(\tau)\} = E(\tau)/(\rho_w S_w L_e)$$

where H is the heat content and:

$$H(T) = \int_{T_0}^{T} c_{pw}(T')dT'$$

Table 2—Covered Electrodes Investigated—Core Diameters Between 1¾ and 6 mm

Designation	d_f/d_w	AWS A5.1	ISO 2560
R1	1.7-1.8	E 6013	E51 3RR 32
R2	1.4-1.5	E 6013	E51 3R 15
R3	1.8-2.1	E 7024	E51 4RR 160 35
B1	1.6-1.9	E 7016	E51 4B 24 (H)
B2	1.5-1.7	E 7016	E51 5B 24 (H)

The curve of H vs. T for pure iron (Ref. 12) was used. This experiment yields $\rho_R(t)$ and E(t) and, hence, the curve of ρ_R vs T. The procedure described here is similar to that described by Halmøy (Ref. 30). Figure 3 shows a typical curve of T_w as a function of time.

The thermal conductivity of the flux material and the product $\rho_f c_{pf}$ were measured by a transient method. A thin electrode (d_w = 2.5 mm = 0.098 in.) was mounted between two contacts, a short (200 ms) high-current (1000 A) pulse was applied, and the temperature of the core wire was determined as a function of time in the manner described above. The use of probes is not necessary in this experiment because the transition regions at the ends remain short.

The wire heated quickly and cooled down by radial heat flow into the coating — Fig. 4. Axial heat flow was negligible. A plane boundary was assumed between core and covering. Furthermore, the core

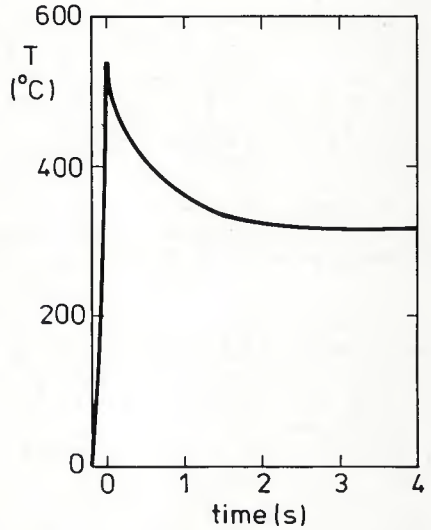

Fig. 4 — Determination of thermal properties of flux material. T = temperature of core. Electrode R1; d_w = 2.47 mm (0.097 in.); d_f = 4.3 mm (0.17 in.); t = 0 at end of pulse; pulse duration — 0.2 s; pulse current — 945 A

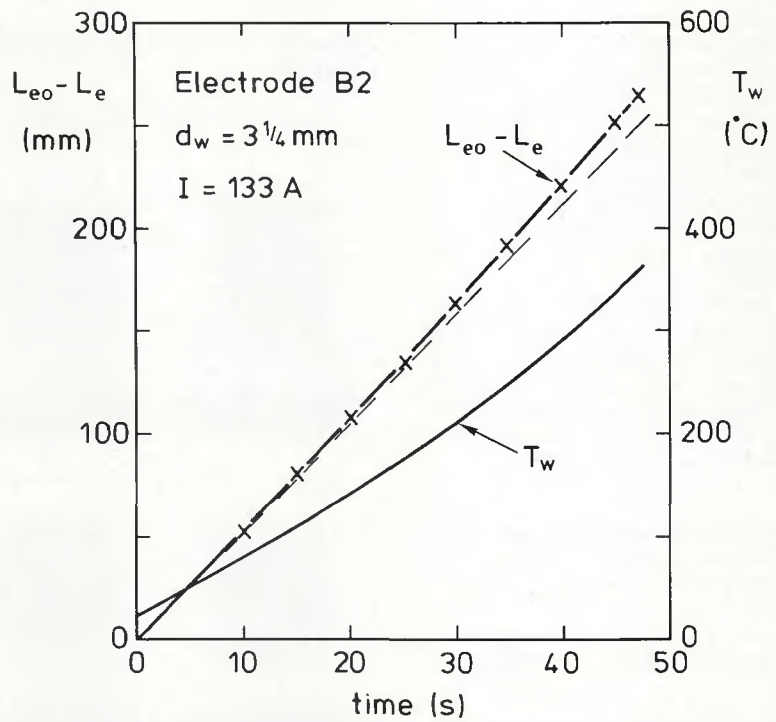

Fig. 3 — Typical curves of molten length and electrode temperature; L_{e0} is the electrode length at t = 0. Melting rate increases from 0.34 g s^{-1} (0.045 lb min^{-1}) at t = 0 to 0.39 g s^{-1} (0.052 lb min^{-1}) at t = 47 s due to Joule heating. Dashes indicate hypothetical curve of $L_{e0} - L_e$ for zero ohmic power; the slope of this curve is proportional to Φ_w

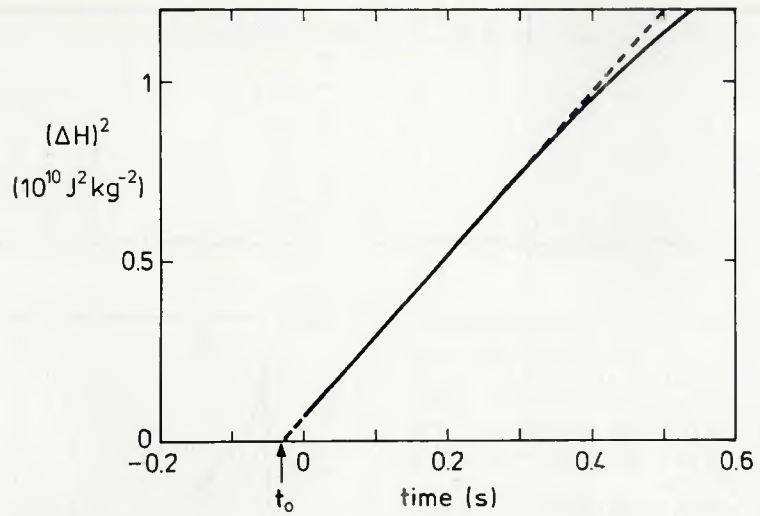

Fig. 5—Plot used in determination of thermal properties of covering materials. Data from same experiment as those in Fig. 4. In this experiment $H(t_0) = 0.31 \times 10^6$ J kg^{-1}

was assumed to heat instantaneously to a homogeneous temperature T_1, at $t = t_0$, and that the coating was at T_0, at that instant. It then followed from the relations given in Ref. 10 and Appendix A that

$$(\Delta H)^2 = \frac{64\,(T_1 - T_0)^2\,(t - t_0)}{\pi\, d_w^2\, \rho_w^2 \{(\lambda_w\, \rho_w\, c_{pw})^{-1/2} + (\lambda_f\, \rho_f\, c_{pf})^{-1/2}\}^2} \qquad (2)$$

where $\Delta H = H(t) - H(t_0)$.

The heat content of the core material, H, followed from the measured temperature, while $H(t_0)$, *i.e.*, the heat content that corresponds to T_1, was equal to the energy supplied per unit core mass during the pulse. The initial slope of a plot as given in Fig. 5, then yielded the product $\lambda_f\, \rho_f\, c_{pf}$. As there was heat flow before the end of the pulse ($t = 0$), it was found that $t_0 < 0$—Fig. 5.

The temperature of electrode and flux became equal and attained a steady value after a few seconds—Fig. 4. The product $\rho_f c_{pf}$ was derived from this steady value, with the masses of electrode and flux and E(t) determined as described above.

Table 3—Temperature-Averaged Values for Thermal Properties of Flux

Electrode	λ_f, W m^{-1} (°C)$^{-1}$	$\rho_f\, c_{pf}$, 10^6 J m^{-3} (°C)$^{-1}$
R1	0.9 ± 0.1	2.1 ± 0.2
R2	0.7	2.4
R3	0.9	1.9
B1	0.9	2.0
B2	1.0	2.0

This method allowed the determination of λ_f and the product $\rho_f c_{pf}$ from a single experiment. Moreover, an actual electrode can be used, although it has to be thin in order to keep the current within reasonable limits. Table 3 gives the results.

High-speed x-ray films of the electrode tip were made at positive and negative polarity for each type of electrode used (1000 pictures/s, d_w = 3¼ mm (0.13 in.), I = 125-160 A). The films were made by E. Oster (RWTH, Aachen). Figure 6 shows a typical sequence.

Derivation of Heat Flow Through Liquid Tip

Thermal power Φ provides the heat to raise the temperature of the metal from T_w to T_{mp}, the heat of fusion, and the power Φ_f which is transferred to the coating in the region adjacent to the melting front. It thus follows that:

$$\Phi(t) = \mu\,(t)\,\{H_{mp} - H\,[T_w(t)]\} + \Phi_f(t) \qquad (3)$$

where H_{mp} is the energy required to convert 1 kg (2.2 lb) of steel at T_0 into 1 kg of molten steel at T_{mp}. The values of T_{mp}, H_{mp}, and H for pure iron (Ref. 12) were used (T_{mp} = 1536°C = 2797°F and $H_{mp} = 1.3 \times 10^6$ J kg^{-1}).

The heat flow rate $\Phi_w = \Phi - \Phi_f$ is related to the measured quantities L_e and T_w by equation (3) and the relation

$$\mu = -\rho_w\, S_w\, dL_e/dt \qquad (4)$$

Since L_e is measured at discrete points of time, it is appropriate to introduce the average value of Φ_w in the interval between t_1 and t_2, $\overline{\Phi}_w(t_1,t_2)$. Equations (3) and (4) give:

$$\overline{\Phi}_w(t_1,t_2) = -\rho_w S_w\{L_e\,(t_2) - L_e\,(t_1)\}/\int_{t_1}^{t_2} \frac{dt}{H_{mp} - H(t)}.$$

The average $\overline{\Phi}_w$ will vary with t if Φ_w does, and $\overline{\Phi}_w = \Phi_w$ if Φ_w is constant. It was found that within the experimental error (≈5%) Φ_w is independent of t for all the electrodes except for those of type R2, where Φ_w decreased by about 15% during the welding time. The values to be given for this electrode refer to $t = 0$ (start of current flow).

Figure 3 shows the hypothetical curve of length melted as a function of time in the absence of Joule heating ($T_w = T_o$ at

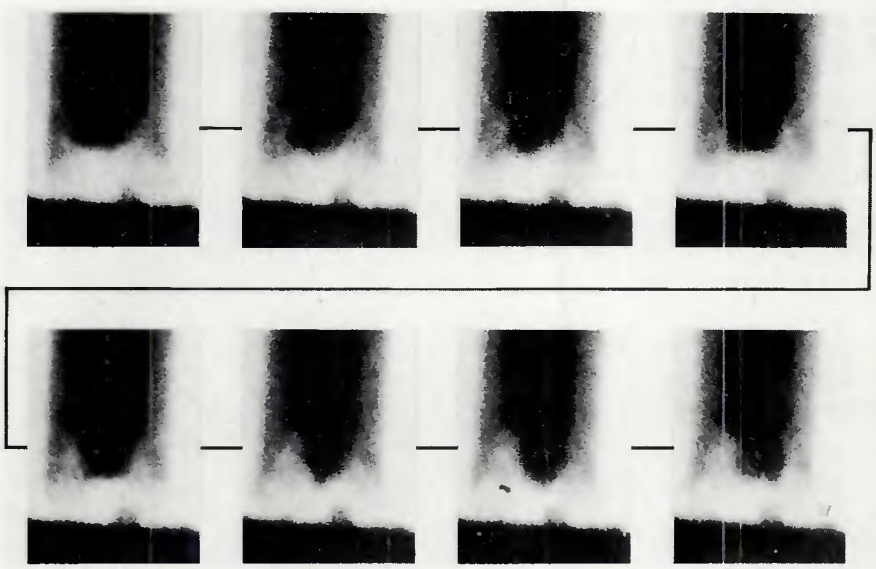

Fig. 6—Sequence from high-speed x-ray film of electrode tip. Framing rate 1000 s^{-1}, electrode R1, positive polarity, d_w = 3.25 mm, d_f = 5.60 mm, I = 141 A

any time). The slope of this curve is proportional to Φ_w; it is, therefore, independent of time for the electrode concerned. On the other hand, the slope of the measured curve increases gradually with time as a result of Joule heating.

Since the slope of the latter curve is proportional to the melting rate, it follows from Fig. 3 that the melting rate increases as a result of Joule heating of the solid metal. The difference between the two curves of length vs. time in Fig. 3 is due to Joule heating. These curves are typical for manual electrodes under normal welding conditions. Consequently, it is seen that Joule heating provides a minor but not entirely negligible part of the total thermal power supplied to the electrode.

The power Φ_f was calculated, as a rule, from:

$$\Phi_f = \pi\, d_w\, \lambda_f\, (T_{mp} - T_o)\, (a_w/a_f)^{1/2} \quad (5)$$

Equation (5) is derived in Appendix B. It is applicable when the depth of penetration of the heat into the covering is small with respect to the thickness of the coating, as was usually the case. When this condition was not fulfilled, then a different relation was used. This relation is also discussed in Appendix B. The diffusivity a_w was taken to be:

$$7.3 \times 10^{-6}\ m^2\ s^{-1}$$

which follows from:

$$\rho_w = 7870\ kg\ m^{-3}$$

and the temperature averages:

$\overline{\lambda}_w = 40\ W\ m^{-1}\ (°C)^{-1}$ and $\bar{c}_{pw} = 700\ J\ kg^{-1}\ (°C)^{-1}$ (Refs. 12-14).

The full set of experimental results is given in Tables 4–9. Positive polarity means electrode positive with respect to workpiece. Figures 7 and 8 show Φ as a function of I. It is seen that Φ varies approximately linearly with I. The slope of the curves for the R1 and B1 electrodes is not very different. This suggests that the physical processes that control the heat flow in the liquid tip are basically the same in the whole range of parameters investigated. Nevertheless, inspection of Tables 4-9 shows that the effects of composition, polarity and diameter on Φ are still large enough to be of practical interest.

The R1 electrode was investigated down to very low current densities. Figure 9 shows the ratio Φ/I. It was seen that Φ/I decreases with increase in I, and becomes constant at high currents. The measurements with the other electrodes were made in the range of higher currents where electrodes are normally used. The results in Tables 4-9 show a tendency for Φ/I to decrease with increase in I.

Table 4—Experimental Results—Electrode R1

d_w, mm	Polarity	I, A	Φ_f, W	Φ, W	Φ/I, V
1¾	+	39	24	133	3.4
2½	+	82	42	259	3.2
3¼	+	30	33	125	4.2
3¼	+	40	35	165	4.1
3¼	+	60	43	236	3.9
3¼	+	81	43	293	3.6
3¼	+	152	55	518	3.4
4	+	153	68	553	3.6
4	+	183	68	648	3.5
5	+	52	54	283	5.4
5	+	103	84	516	5.0
5	+	164	84	661	4.0
5	+	220	84	833	3.8
5	+	250	84	911	3.6
5	+	285	84	1055	3.7
5	+	345	84	1224	3.6
6	+	258	101	1050	4.1
6	+	334	101	1251	3.8
1¾	–	40	24	130	3.2
2½	–	82	42	250	3.0
3¼	–	83	44	259	3.1
3¼	–	120	55	358	3.0
3¼	–	155	55	481	3.1
4	–	153	68	529	3.5
4	–	183	68	620	3.4
5	–	220	84	796	3.6
5	–	251	84	903	3.6
5	–	286	84	1002	3.5
6	–	258	101	874	3.4
6	–	335	101	1196	3.6

Table 5—Experimental Results—Electrode R2

d_w, mm	Polarity	I, A	Φ_f, W	Φ, W	Φ/I, V
2½	+	71	34	286	4.0
2½	+	87	34	327	3.8
3¼	+	88	44	355	4.0
3¼	+	123	55	470	3.8
3¼	+	153	55	561	3.7
5	+	205	66	804	3.9
5	+	246	84	963	3.9

Table 6—Experimental Results—Electrode R3

d_w, mm	Polarity	I, A	Φ_f, W	Φ, W	Φ/I, V
2½	+	102	42	326	3.2
2½	+	123	42	350	2.8
3¼	+	164	55	492	3.0
5	+	229	84	787	3.4
3¼	–	129	55	403	3.1
3¼	–	165	55	474	2.9
5	–	231	84	765	3.3
5	–	332	84	1056	3.2

Temperature of Surface of Pendent Drop

Particularly surprising is the small effect of polarity on Φ. The processes occurring at a cathode and those occurring at an anode are essentially different (Ref. 15), so that one expects a strong dependence of V_0 and, consequently, of Φ, on polarity, contrary to the experimental results. Therefore, a discussion of the heating of the tip surface is required.

The temperature of the tip surface will adjust itself such that the incoming power is carried away by radiation, evaporation, and by convection and thermal conduction in the liquid metal. For the purpose

Table 7—Experimental Results—Electrode B1

d_w, mm	Polarity	I, A	Φ_f, W	Φ, W	Φ/I, V
2½	+	87	42	305	3.5
2½	+	102	42	337	3.3
3¼	+	95	55	350	3.7
3¼	+	124	55	409	3.3
4	+	122	68	462	3.8
4	+	183	68	587	3.2
5	+	228	84	782	3.4
3¼	−	93	55	367	3.9
3¼	−	125	55	399	3.2
4	−	114	68	456	4.0
4	−	150	68	509	3.4
4	−	186	68	633	3.4
5	−	192	84	770	4.0
5	−	230	84	952	4.1

Table 8—Experimental Results—Electrode B2

d_w, mm	Polarity	I, A	Φ_f, W	Φ, W	Φ/I, V
2½	+	71	42	287	4.0
2½	+	102	42	362	3.6
3¼	+	87	55	361	4.1
3¼	+	133	55	492	3.7
5	+	204	84	791	3.9
5	+	244	84	960	3.9

Table 9—Experimental Results—Bare Electrodes

d_w, mm	I, A	Φ, W	Φ/I, V	Gas[a]
2	51	220	4.3	Ar
2	77	342	4.4	Ar
2½	51	199	3.9	Ar
3¼	102	398	3.9	Ar
3¼	128	523	4.1	Ar
5	230	961	4.2	Ar
5	255	1099	4.3	Ar
2	52	250	4.8	Ar/CO_2
2	75	339	4.5	Ar/CO_2
3¼	103	473	4.6	Ar/CO_2
3¼	143	620	4.3	Ar/CO_2
5	205	1006	4.9	Ar/CO_2
5	253	1120	4.4	Ar/CO_2

(a) Shielding gas either Ar (18 − L/min) or Ar/CO_2 (Ar − 10 L/min, CO_2 − 1½ L/min); positive polarity.

of obtaining orders of magnitude of the terms in equation (1) we may neglect Joule heating and the term Φ_f in (3), which yields $\mu = \Phi/H_{mp}$. It then follows from equation (1) that

$$V_0 \approx \frac{\Phi}{I}\left\{1 + \frac{c_{pl}(\bar{T}_{dr} - T_{mp})}{H_{mp}}\right\} + \frac{\Phi_L}{I} \qquad (6)$$

Anode (Cathode) Power V_o

Consider that the arc is attached to the anode on an SMAW electrode in the anode jet dominated mode, as described by Sanders and Pfender (Ref. 16). Their work shows that the anode is then heated mainly by electron absorption, while there are smaller contributions by thermal conduction and radiation from the plasma. They also give expressions for the electron heat flux at the anode for positive and for negative anode falls.

The anode will be negative with respect to the adjacent plasma if the random electron current density, $j_r = \frac{1}{4} n_e v_e e$, at the edge of the space charge sheath, is less than the current density at the anode surface (Ref. 17) where n_e is the electron number density, $v_e = (8k T_e/\pi m_e)^{1/2}$ the mean thermal velocity of the electrons, T_e is the electron temperature, and e and m_e are the electron charge and mass, respectively.

There are, to the authors' knowledge, no measured data available on T_e and n_e in SMAW arcs, but results (T_e = 7000 K, $n_e = 10^{22}$ m^{-3}) for the metal vapor plasma in a plasma-GMA arc (Ref. 33), may be used to obtain orders of magnitude. An analysis based on these data (Ref. 18) shows that $j_r \approx 40 A/mm^2$, while the current density at the anode surface, j_A, is about 20 A/mm^2. Therefore, the anode fall may be assumed to be negative. Considering the electron heat flux only, we have from the literature (Ref. 16):

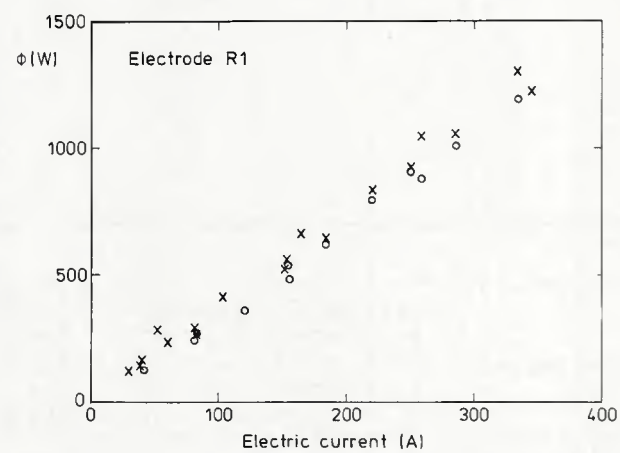

Fig. 7—Thermal power transferred through liquid tip. Rutile electrode; d_w from 1¾ to 6 mm (0.07 to 0.24 in.). X—electrode positive; O—electrode negative

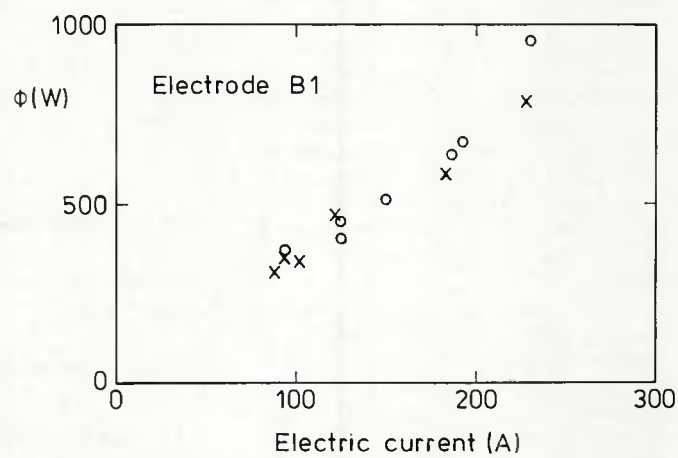

Fig. 8—Same as Fig. 6 but for basic electrode

$$V_o = 3.2\ k\ T_e/e + \varphi$$

where φ is the work function (4.4V) for iron (Ref. 13). We thus obtain $V_o \approx 6$ V. Analysis of GMA experiments yielded 5.5 V (Refs. 19-20) and 6.0 ± 0.5 V (Ref. 9).

The radiation loss at temperatures close to the boiling point amounts to about 5 W/mm^2; this corresponds to 0.2 V with j_A as given above and is neglected here. The evaporation loss is controlled by the diffusion of metal vapor through the boundary layer in front of the drop surface.

An estimate of this term would require an analysis of the boundary layer, which is outside the scope of this paper. Neglecting this loss term for the moment, we can make an estimate of $\overline{T}_{dr}$. Equation (6) with $\Phi_L = 0$, V_o as above, and $\Phi/I = 3.5$ V, a typical value obtained from the experiments, gives $\overline{T}_{dr} \approx 2700$ °C (4900 °F), *i.e.,* close to the boiling point, $T_b = 2862$ °C = 5184 °F (Ref. 12).

The temperature of the anode surface is bound to be well above $\overline{T}_{dr}$. Consequently, the hypothesis of zero evaporation loss must be incorrect. Although the value of this loss is not known, it is clear that it will increase with increase in surface temperature. We hypothesize that the temperature of the anode surface, which might still be close to T_b, is stabilized by the evaporation of metal (Ref. 21). Therefore, this temperature is insensitive to the exact value of V_o, as long as V_o is above a certain minimum value, *i.e.,* about 5.5 V in the system discussed here.

The mechanism of heat generation at a cathode surface is extremely complicated (Ref. 15), and no data on V_o for this process have been found in the literature. On the other hand, the argument on the stabilization of the surface temperature, as given above, remains the same. Consequently, the assumption that V_o is above 5.5 V for positive and negative polarity explains the absence of a major influence of polarity on Φ.

As an approximation, the difference between the temperature of the anode (cathode) surface and the melting point will be taken as 1000 °C (1800 °F).

It must be noted that the effect of polarity on the melting rate in flux-shielded processes is not always as small as was observed in the experiments described here. Investigations of the submerged arc welding (SAW) process (Ref. 22) showed that polarity can have a distinct effect, depending on flux composition and current strength.

Mechanism of Heat Flow through Liquid Tip

The experiments show that a large part of the heat generated at the tip surface is transferred through the drop to the solid metal. This heat transfer is due to thermal conduction, or to fluid flow, or to both. These processes are now discussed in order to explain the experimental results, in particular the linear dependence of Φ on I.

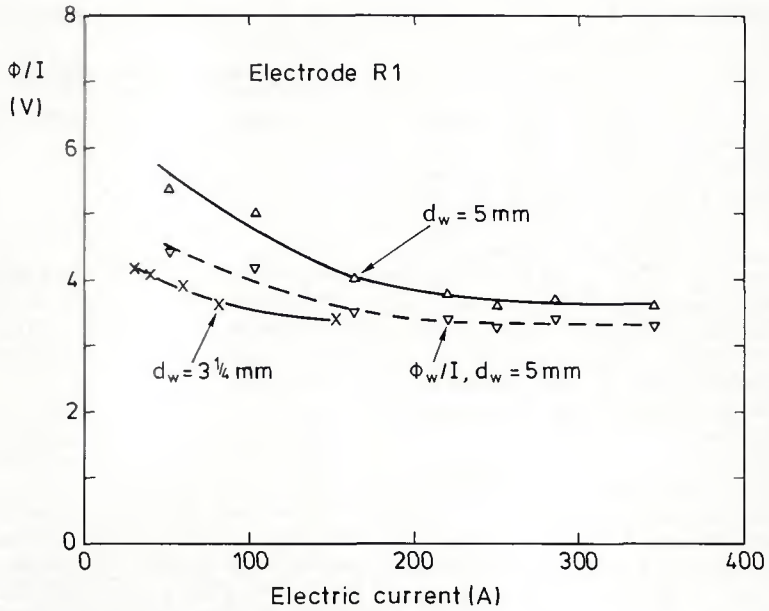

Fig. 9—Thermal power per ampere as a function of current. Also shown is a curve of $\Phi_w/I = (\Phi - \Phi_f)/I$ in order to show effect of heat flow into covering

Possible causes of fluid flow are electromagnetic forces, the buoyancy force, and the force due to a gradient in the surface tension, γ.

The electromagnetic (Lorentz) force is due to the interaction of the electric current with its own magnetic field. It will generate fluid flow if the electric current diverges or converges within the pendent drop (Refs. 9, 15, 23, 24). The order of magnitude of the force on the drop is given by $F_L \approx \mu_0 I^2/4\pi$, where μ_0 is the permeability of vacuum.

The buoyancy force, F_b, is due to heating of the metal at the bottom of the drop. Its order of magnitude is $F_b \sim L^3 \rho_l$ g α ΔT_s (Ref. 25), where L is a typical length, g the gravity constant, α the expansion coefficient, and ΔT_s the difference between the temperature of the anode (cathode) surface and the melting point.

A gradient in γ will be caused by the segregation of oxygen, which is strongly surface-active in iron, while the degree of segregation is temperature-dependent (Refs. 26, 27). The addition of 0.1% of oxygen to pure iron lowers γ from 1.9 to 1.3 Nm^{-1} at 1650 °C (3000 °F) (Ref. 26). Furthermore, the surface tension of any pure metal is temperature-dependent. The force on the surface per unit area is equal to grad γ and the force on the drop as a whole

$$F_\gamma \approx L^2 \text{ grad } \gamma \approx L\ \Delta\gamma$$

where $\Delta\gamma$ is the difference in γ between top and bottom, estimated to be the order of 0.1 Nm^{-1}.

The relative importance of the three forces discussed was estimated with the average properties given in Table 10, with L and I in the ranges usual for manual electrodes. It was found that F_L will be the dominant force, but that F_γ and F_b can attain values of up to 30% of F_L.

Discussion of the model below considers heat transfer by conduction, and by convection due to the electromagnetic force. The treatment of this force is only approximate, so that it would be meaningless to include the other, smaller, forces as well.

The electromagnetically induced fluid flow will be in the direction of decreasing current density, *i.e.,* in the direction of widening path of the electric current. The current density in the electrode is around 15 A mm^{-2} (10^4 A/in.^{2}). It is expected to have roughly the same value on the anode surface and to be higher in a

Table 10—Values Used for the Properties of Liquid Iron (Ref. 13)

Property	Value
ρ	6500 kg m^{-3}
c_p	800 J kg^{-1} (°C)$^{-1}$
λ	40 W m^{-1} (°C)$^{-1}$
α	1.3 × 10^{-4} (°C)$^{-1}$
ν	0.6 × 10^{-6} m^2 s^{-1}
a	8 × 10^{-6} m^2 s^{-1}
ρ_R	1.4 × 10^{-6} Ω m

cathode spot (Ref. 15). Consequently, the direction of the flow is uncertain at positive polarity.

At negative polarity, the flow in the region which carries the electric current will be directed from the cathode surface to the solid metal. The electromagnetically induced flow velocity, u_L, is proportional to I if the Reynolds number, $Re = u_L L/\nu_l$, is large ($Re \gg 1$), and proportional to I^2 if $Re \ll 1$ (Ref. 9). In the treatment given below, the fluid flow at both polarities is assumed to be as for negative polarity. The essential features of the model remain the same if the flow direction is reversed. Further assumptions are (see Fig. 10):

1. The height, h, of the pendent drop is constant, and it is a few mm. We thus consider either a drop of average size, or a situation where there is a continuous outflow of small drops from the pendent drop.

2. Heat is generated at the lower surface (z = h), where $T = T_{mp} + \Delta T_s$, and ΔT_s is constant.

3. The hot liquid is cooled to T_{mp} at the solid-liquid boundary and gives off the excess heat to the solid.

4. The whole electrode is moving into the positive z-direction at a velocity u_e, while the fusion boundary remains in a fixed position, taken as z = 0. The effects of Joule heating, and of the heat flow Φ_f are neglected, so that

$$u_e = \Phi/(S_w \rho_w H_{mp}) \qquad (7)$$

cf. Eq. (3). The omission of the Joule heating is the essential difference between the model developed for the gas metal arc (GMA) process (Ref. 9) and the model developed here.

5. The spatial distribution of the temperature does not vary in time.

The temperature in the center is then given by

$$-u \frac{\partial T}{\partial z} = a_l \frac{\partial^2 T}{\partial z^2} \qquad (8)$$

where $u = u_L - u_e$ is the net upward velocity (u_L and u_e are positive). Boundary conditions are that $T = T_{mp}$ at z = 0, and $T = T_{mp} + \Delta T_s$ at z = h. The solution to equation (8) is:

$$T(z) = T_{mp} + \Delta T_s \frac{1 - \exp(-u\, z/a_l)}{1 - \exp(-u\, h/a_l)} \qquad (9)$$

The expression $Pe = u\, h/a_l$ in equation (9) is the Péclet number; it is frequently used in heat transfer calculations (Ref. 25). This number gives, approximately, the ratio of the heat flux by convection ($u\, \rho_l\, c_{pl}\, \Delta T_s$) to the heat flux by conduction ($\approx \lambda_l\, \Delta T_s/h$).

Heat transfer is primarily by conduction if Pe is small, and primarily by convection if Pe is large. Figure 11 shows the general shape of the temperature profile in the region of upward flow. The rate of heat flow into the solid, *i.e.*, the power Φ is proportional to the slope of this curve at z = o. It is given by:

$$\Phi = \lambda_l\, S^* \left(\partial T/\partial z\right)_{z=0} = \frac{\lambda_l\, S^*\, Pe\, \Delta T_s}{h\,\{1 - \exp(-Pe)\}} \qquad (10)$$

where S* is the cross-sectional area of the region of upward flow.

Limiting Cases

Heat Transfer Primarily Conduction. Here $Pe \ll 1$. Equation (10) then gives:

$$\Phi \approx \lambda_l\, S^*\, \Delta T_s/h.$$

In order to obtain the linear dependence of Φ on I, one would have to assume that $S^*/h \propto I$. There is no physical basis for this assumption.

Heat Transfer Primarily by Convection. Equations (7) and (10) give:

$$\Phi \approx \frac{S^*\, u_L\, \rho_l\, c_{pl}\, \Delta T_s}{1 + \dfrac{S^*\, \rho_l\, c_{pl}\, \Delta T_s}{S_w\, \rho_w\, H_{mp}} - \exp(-Pe)} \qquad (11)$$

The exponential term vanishes when $Pe \gg 1$, so that Φ is then proportional to u_L.

Agreement With Experimental Results

In order to obtain agreement with the experimental results, one has to assume that u_L is proportional to I. This implies that $Re \gg 1$, as was mentioned. With $\Phi/I = 3.5$ V, $\Delta T_s = 1000$ °C, $I/S_w = 15$ A/mm^2 (10^4 A in.$^{-2}$) as typical values and assuming that $S^*/S_w = 0.5$, we can determine that u_L is in the order of a few centimeters per second (≈ 1 in./s^{-1}). The Reynolds number is then between 10 and 100; this is consistent with the assumption that u_L is proportional to I. The magnetic Reynolds number, $R_m = \mu_0\, L\, u_L/\rho_{RI}$ (Ref. 28) is then of the order of 10^{-4} so that the back e.m.f. generated by the fluid flow is negligible.

The ratio u_L/I is found to lie between 10^{-4} and 10^{-3} m s^{-1} A^{-1}. GMA experi-

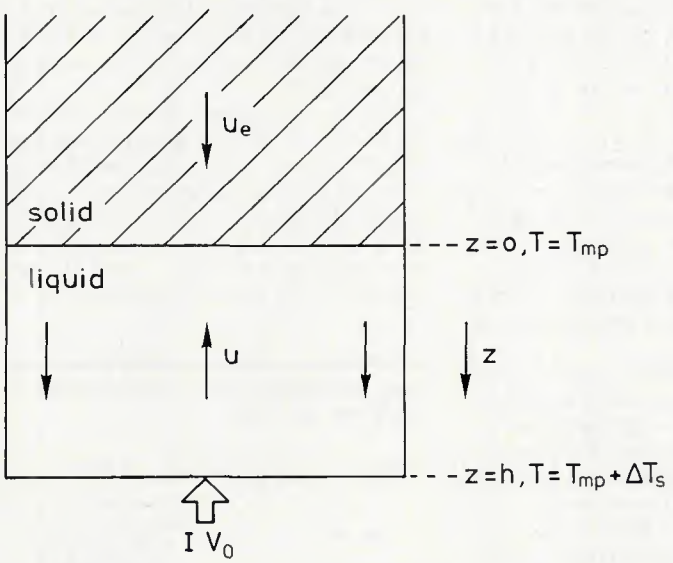

Fig. 10—Illustration of heat transfer in pendent drop

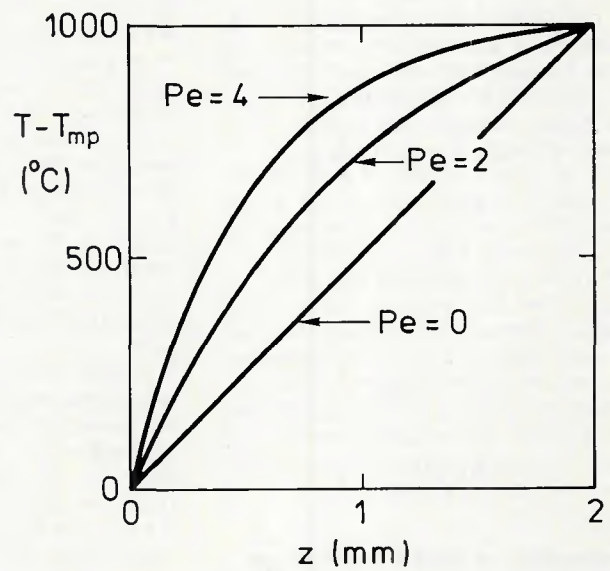

Fig. 11—Illustration of temperature distribution in pendent drop. Profiles given by equation (9) are drawn for ΔT_s = 1000 °C (1800 °F), h = 2 mm, $a = 8 \times 10^{-6}$ m^2 s^{-1}, with Pe = 0 (u = 0), Pe = 2 (u = 8 mm s^{-1}), and Pe = 4 (u = 16 mm s^{-1})

ments (Ref. 9) with 1.2 mm (0.047 in.) diameter mild steel electrodes gave $u_L/I \approx 10^{-3}\ m\ s^{-1}\ A^{-1}$. This ratio is expected to decrease with increased d_w, so that these results compare favorably.

Since $Pe/Re = \nu_l/a_l = 0.075$, it follows that Pe lies between 1 and 10. Consequently, the exponential term in the denominator in equation (11) is not necessarily negligible. If it is not, then equation (11) gives an increase in Φ/I with decrease in Pe, *i.e.*, with decrease in I (Pe is proportional to $u_L - u_e$, and u_L and u_e are proportional to I). Figure 9 shows that this behavior is in fact observed.

Equation (11) thus accounts for the experimental result that Φ/I is constant at higher currents, and decreases as I is lowered—Fig. 9. It also follows from the model that $\Phi/I \rightarrow V_0$ ($\approx 6V$) as $I \rightarrow 0$. The assumption of constant ΔT_s has then to be dropped. This point further confirms the increase in Φ/I as I decreases.

The experimental results show that Φ/I tends to decrease slightly with increase in I in the range of current densities normal for SMA welding. Therefore, the exponential term in equation (11), which represents the effect of thermal conduction, is small but not completely negligible. Since this decrease in Φ/I is about 5 to 10%, the Péclet number must be close to 3, because $\exp(-3) = 0.05$. In other words, at normal current densities the conditions for convection-dominated heat transfer are fulfilled, but only just. A decrease in Pe from 3 to 2 would imply an essential change in the mechanism of heat transfer.

Figures 12 and 13 show Φ/I as a function of d_w. The results for the basic electrodes are not shown in Fig. 13. They lie between the curves for R2 and R3 in Fig. 13. The covered electrodes show, in general, an increase in Φ/I with increase in d_w. The model does not account for this result. Calculation of these curves requires knowledge of the dependence of u_L on d_w. This, in turn, requires knowledge of the dependence of the current-carrying area on the tip surface on d_w and I. This information is, to the authors' knowledge, still lacking. Furthermore, the effect might be due to the buoyance force or to surface tension streaming.

Figure 12 contains points derived from results obtained by Wilson *et al.* in SAW experiments (Ref. 29). The closeness of these curves and those for the SMA process suggests that the same processes of heat transfer are operative in the two systems.

Figure 13 also shows points obtained with bare electrodes at positive polarity. Reproducible results could not be obtained with negative polarity. It is seen that Φ/I is distinctly higher than for covered electrodes, as was also observed by Lefring (Ref. 7). This suggests that the covering absorbs a sizable fraction of the heat supplied to the liquid metal. However, this hypothesis has to be rejected for the following reasons:

1. X-ray films show that, although the pendent drop is constantly in motion and occasionally touches the surrounding cup, there is certainly not a good thermal contact; similar results were obtained by Becken (Ref. 2) and Klimant (Ref. 3).

2. Experiments with R1 and B1 electrodes (Table 11) show that Φ is independent of the thickness of the coating for a given flux composition.

We have no explanation for the observed difference between covered and bare electrodes. However, there is a possibility that the difference is due to the fact that the anode area is more steady on a bare electrode in argon than on a covered electrode where it wanders due to the motion of slag. Film images (Ref. 2) show that slag prevents arc attachment. An unsteady anode implies an unsteady pattern of fluid flow.

Figure 13 also shows a point for mild steel wire in GMA welding. It is seen to lie within the range covered by the manual electrodes.

Heat Flow Into the Covering

The covering is heated by thermal conduction from the solid part of the wire, and cooled at its outer surface by radiation and natural convection. Joule heating by current flow through the covering is negligible, because the resistivity of the flux material is several orders of magnitude higher than the resistivity of iron (Ref. 31). Therefore, the electric current in the covering is negligible.

The temperature within the flux is given by:

$$\frac{\partial T}{\partial t} = a_f \nabla^2 T \qquad (12)$$

together with appropriate boundary conditions. The expression $\nabla^2 T$ is of the order of magnitude $\Delta T/L^2$, where L is the thickness of the coating, and ΔT the temperature difference across it. Orders of magnitude are L = 1 mm (0.04 in.), $a_f = 0.4 \times 10^{-6}\ m^2 s^{-1}$, and $\partial T/\partial t \approx 10\ °C\ s^{-1}$, which gives $\Delta T = 25\ °C$ (45 °F) as a typical value.

Equation (12) was also solved numerically for the region where the temperature profile (Fig. 2) is flat. The flux properties and $\rho_R(T)$ were taken as measured, and c_{pw} (T) as in the literature (Ref. 12). Radiative and convective losses to the surroundings (see below) were accounted for. The difference ΔT was found to increase with time. Table 12 gives ΔT for two typical cases near the end of the welding time (also see Fig. 3).

The covering absorbs a part of the ohmic power, and its thickness influences the melting rate via T_w (Table 11). The effect is not, however, of major impor-

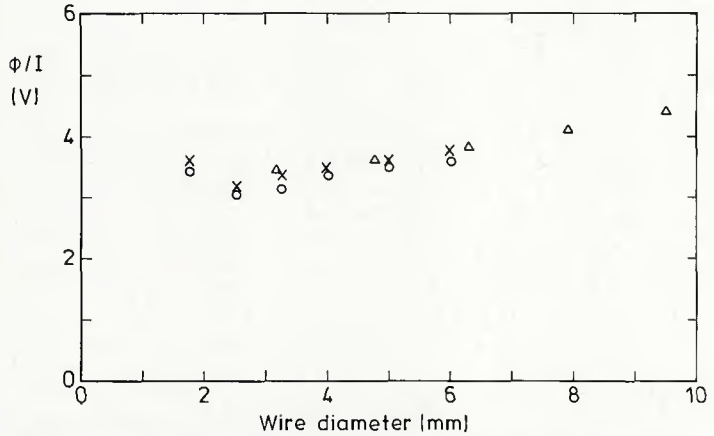

Fig. 12—Dependence of thermal power per ampere on electrode diameter. Values of Φ/I at the highest current used. X—Electrode R1, positive polarity; O—Electrode R1, negative polarity; Δ—derived from results of SAW experiments obtained by Wilson et al *(Ref. 29)*

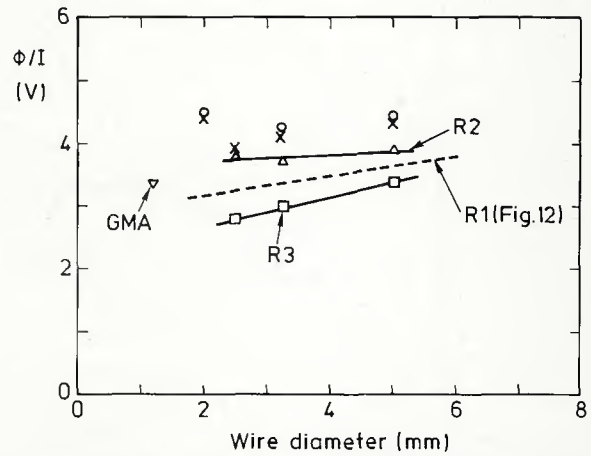

Fig. 13—Same as Fig. 11 but with positive polarity. X—bare electrodes in Ar; O—bare electrodes in Ar/CO_2; Δ—electrode R2; □—electrode R3; ▽—GMA, mild steel in Ar, $I \rightarrow 0$ (Ref. 9)

tance, because ohmic heating is not the dominant heat source.

The heat flow Φ_f from the core into the covering in the region adjacent to the melting front will raise the temperature by a few hundred degrees. As it is unlikely that there is a large heat flow from the liquid metal directly into the covering, it follows that the heat required to decompose and melt the covering is provided mainly by the arc.

The amount of flux used is of the order of a few milligrams per amp per second. The power per unit length in the arc is equal to I E, where E is the axial electric field strength ($\sim$1 V mm^{-1} = 25 V in.$^{-1}$). The cup surrounds a part of the arc and absorbs the power generated in the plasma it encloses. The length of the cup is usually a few mm, and it follows that the energy absorbed per unit mass of flux material is of the order of 10^6 J kg^{-1} which is the right order of magnitude.

Table 11—Effect of Covering Thickness on Heat Flow in Wire Tip[a]

Type	d_f, mm	I, A	Φ, W	μ_{av}/I, mg s^{-1} A^{-1}
R1	6.3	207	706	2.84
R1	6.6	207	718	2.77
R1	6.9	207	719	2.73
B1	6.3	169	540	2.46
B1	6.6	169	544	2.42
B1	6.9	169	542	2.39

(a) Positive polarity, d_w = 4 mm; μ_{av} is the time average of μ, taken over the total welding time.

Table 12—Temperature Difference across Covering after 45 s

Electrode	d_w, mm	d_f, mm	I, A	T_w (exp.), °C	T_w (calc.), °C	ΔT (calc.), °C
R1	3.20	5.6	152	541	551	74
B2	3.21	5.3	133	336	365	28

Survey of Thermal Processes

Concern here is with the processes of heat generation and heat transfer in a typical electrode, *i.e.*, B2, d_w = 3¼ mm, I = 133 A.

The length L_e and ρ_R were measured as functions of t, and ρ_R gives T_w. The following quantities were calculated from these results:

1. The ohmic power developed in the solid wire:

$$P_\Omega(t) = I^2\, \rho_R(t)\, L_e\,(t)/S_w$$

2. The ohmic power carried away by the steel through the melting front:

$$P_{\Omega w}(t) = u_e(t)\, \rho_w\, S_w\, H(t)$$

3. The ohmic power $P_{\Omega f}$ similarly carried away by the flux, where Φ_f is not considered. It was assumed that the flux has the same temperature as the core, so that

$$P_{\Omega f}(t) = u_e\,(t)\, \rho_f\, S_f\, c_{pf}\, \{T_w\,(t) - T_0\}$$

4. The power lost by radiation (P_{rad}), and that lost by convection (P_{conv}) from the outer surface of the covering to the surroundings,

$$P_{rad}\,(t) = \pi\, d_w\, L_e\,(t)\, \sigma\, \{T_w{}^4\,(t) - T_0{}^4\}$$

and:

$$P_{conv}\,(t) = \pi\, d_w\, L_e\,(t)\, \beta\, \{T_w\,(t) - T_0\}$$

where σ is the Stefan-Boltzmann constant and β is the heat transfer coefficient for natural convection. The typical value β = 10 W m^{-2} (°C)$^{-1}$ = 0.004 W in.$^{-2}$ (°F)$^{-1}$ (Ref. 32) was used.

Figure 14 shows the powers discussed above. It is seen that the bare wire and the covering absorb roughly equal parts of the ohmic energy. The energy developed by Joule heating during the welding time (τ) is given by:

$$Q_\Omega = \int_0^\tau P_\Omega\,(t)dt$$

The energies $Q_{\Omega w}$, $Q_{\Omega f}$, Q_{rad}, and Q_{conv}, defined in the same way, were also calculated.

The major part of the heat is provided by anode or cathode processes at the tip, where a power IV_0 is generated. A part of this power is lost by evaporation (Φ_{ev}), another part is absorbed by the liquid metal ($\mu\, c_{pl}\, (\overline{T}_{dr} - T_{mp})$). The remainder, Φ, is transferred to the solid metal. The experiments give no information about Φ_{ev}. Gas metal arc experiments with steel (Refs. 9, 19-20) gave $V_0 \approx 6$V, which value is used as an approximation. The difference $\overline{\Delta T} = \overline{T}_{dr} - T_{mp}$ is estimated to be between 700 and 1200 °C (1260 and 2160 °F). A part of Φ is transferred to the coating (Φ_f). The energy absorbed by the solid wire is equal to $Q_w = \Phi_w \tau + Q_{\Omega w}$.

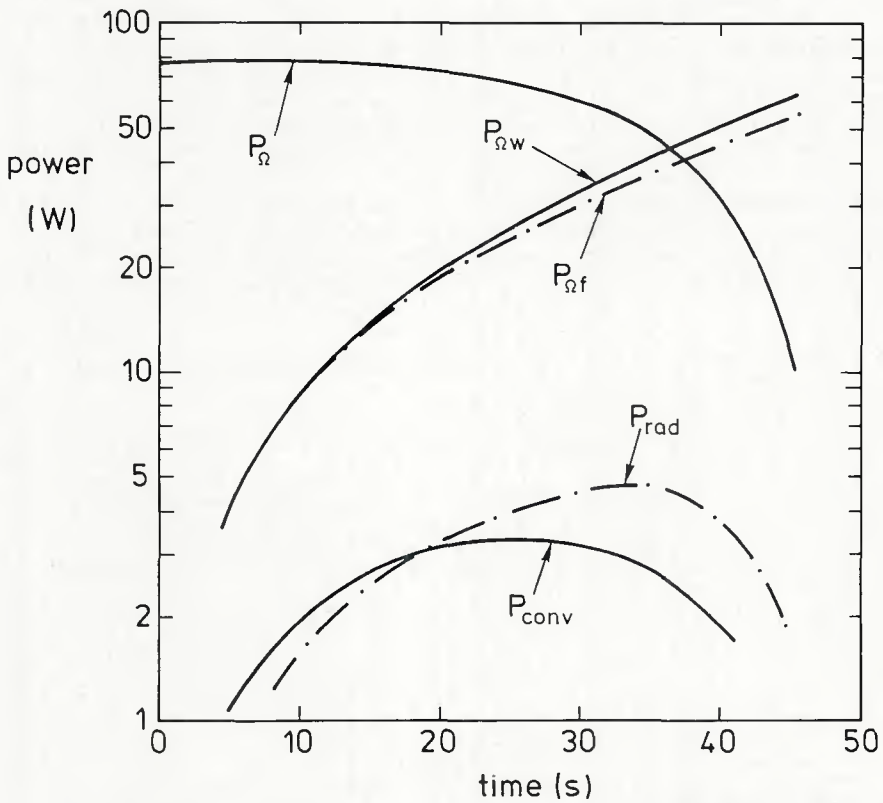

Fig. 14—Rate of generation of Joule heat in solid core, and rates of transfer of this heat through surface of coating and fusion boundary. Decrease in P_Ω, P_{rad} and P_{conv} is caused by decrease in L_e

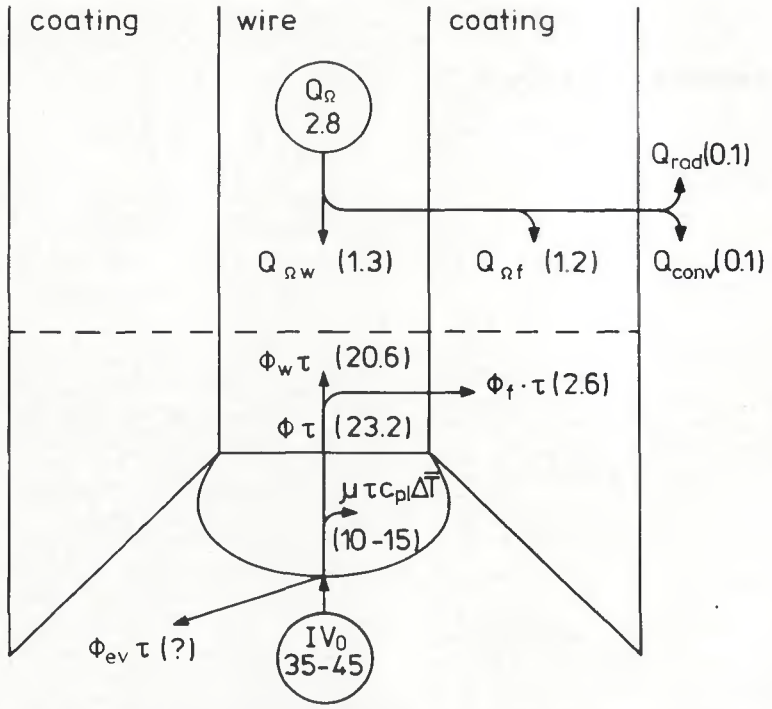

Fig. 15 — Thermal energies transferred in electrode during welding. Electrode B2, d_w = 3.21 mm (0.126 in.), d_f = 5.3 mm (0.21 in.), I = 133 A, τ = 47.2 s, length melted off — 265 mm. Energies in kJ (1 kJ = 0.24 kilocalories), accuracy generally 0.1 kJ

Figure 15 surveys the various quantities of interest. It is to be noted that the values were derived from experimental results. Joule heating provides 6% of the energy supplied to the metal core in this case. Heat losses to the surroundings are small.

Conclusions

The dominant processes of heat generation in covered electrodes are cathode or anode processes occurring at the electrode tip. A part of the heat thus generated is lost by evaporation, the liquid metal absorbing the remainder. The liquid metal, in turn, transfers heat to the solid metal, which melts as a result.

The heat flow rate and, consequently, the melting rate, vary linearly with the electric current. Electromagnetically induced fluid flow broadly accounts for the transfer of heat through the liquid tip.

The requirement that the coating must not be overheated imposes a limit on the electric current. As a result, SMA welding is carried out in the current range where Joule heating provides only a minor part of the total heat supplied.

The temperature difference across a covering of normal thickness is small.

The melting rate per ampere of a covered electrode is comparable with that of a GMA welding wire in the limit of zero Joule heating, *i.e.*, at low current and/or extension length.

Acknowledgments

The authors are indebted to F.J. du Chatenier, H.K. Kuiken, B.A.M. Ross, G.W. Tichelaar and F.F. Westendorp for help and comments during the work.

References

1. Boniszewski, T. 1979. Manual metal arc welding, old process, new developments. *The Metallurgist and Materials Technologist* 11(10):567-574; 11(11):640-643; 11(12):697-705.

2. Becken, O. 1970. Werkstoffübergang bei Schweisselektroden. Schriftenreihe. *Schweissen und Schneiden,* 1. Jahrgang, Bericht 19.DV5 Düsseldorf.

3. Klimant, U. 1967. Beitrag zum Werkstoffübergang beim Lichtbogenschweissen mit dick umhüllten Elektroden. Thesis. Aachen: RWTH.

4. Essers, W. G., Jelmorini, G., and Tichelaar, G. W. 1971. Metal transfer from coated electrodes. *Metal Constr. and Brit. Weld. J.* 3:151-154.

5. Wegrzyn, J. 1969. *The covered electrode arc.* IIW doc. 212-166-69.

6. Lancaster, J. F. 1971. The transfer of metal from coated electrodes. *Metal Constr. and Br. Weld. J.* 3:370-373.

7. Lefring, L. 1930. Einfluss der Schweissstrombedingungen bei der elektrischen Lichtbogenschweissung von weichem Flussstahl. *Forschungsarbeiten auf dem Gebiete des Ingenieurswesens,* VDI Berlin, Heft 332:1-53.

8. Ter Berg, J., and Larigaldie, A. 1952. Melting rate of coated electrodes. *Welding Journal* 31(5):268-s to 271-s.

9. Waszink, J. H., and Van den Heuvel, G. J. P. M. 1982. Heat generation and heat flow in the filter metal in GMA welding. *Welding Journal* 61(8):269-s to 282-s.

10. Carslaw, H. S., and Jaeger, J. C. 1959. *Conduction of heat in solids,* 2nd ed., Chap. 2. Oxford: Clarendon Press.

11. Waszink, J. H., and Van den Heuvel, G. J. P. M. 1979. Measurements and calculations of the resistance of the wire extension in arc welding. *Proc. Int. Conf. on Arc Physics and Weld Pool Behaviour, London,* pp. 227-239. Abington, Cambridge: The Welding Institute.

12. Hultgren, R., Desai, P. D., Hawkins, D. T., Gleiser, M., Kelley, K. K., and Wagman, D. D. 1973. *Selected values of the thermodynamic properties of the elements.* Metals Park, Ohio: American Society for Metals.

13. Smithells, C. J., and Brandes, E. A. 1976. *Metals reference book,* 5th ed. London: Butterworths.

14. Touloukian, Y. S., Powell, R. W., Ho, C. Y., and Klemens, P. G. 1978. *Thermophysical properties of matter,* Vol. 1. New York: IFI/Plenum.

15. Pfender, E. 1978. Electric arcs and arc gas heaters. Chap. 5 of *Gaseous Electronics,* eds. M. N. Hirsh and H. J. Oskam, vol. 1: *Electrical discharges.* New York: Academic Press.

16. Sanders, N. A., and Pfender, E. 1984. Measurement of anode falls and anode heat transfer in atmospheric pressure high intensity arcs. *J. Appl. Phys.* 55(3):714-722.

17. Dinulescu, H. A., and Pfender, E. 1980. Analysis of the anode boundary layer of high intensity arcs. *J. Appl. Phys.* 51(6):3149-3157.

18. Waszink, J. H., and Graat, L. H. J. 1983. Experimental investigation of the forces acting on a drop of weld metal. *Welding Journal* 62(4):108-s to 116-s.

19. Jelmorini, G., Tichelaar, G. W., and Van den Heuvel, G. J. P. M. 1977. *Droplet temperature measurements in arc welding.* IIW-doc. 212-411-77.

20. Van den Heuvel, G. J. P. M., Jelmorini, G., and Tichelaar, G. W. 1978. Messung der Tropfentemperatur im Schweisslichtbogen und ihre Bedeutung in der Praxis. *DVS Ber.* 50 DVS, Düsseldorf: 165-171.

21. T. W. Eagar suggested evaporation as the mechanism which stabilizes the drop temperature during a discussion at the 1982 AWS Convention, Kansas City.

22. Eichhorn, F., Felleisen, R., and Kerkmann, M. 1978. Einfluss der Energieeinbringung auf den Verfahrensablauf beim Unterpulverschweissen mit Drahtelektrode. *DVS Ber.* 50, DVS, Düsseldorf:158-164.

23. Maeker, H. 1955. Plasmaströmungen in Lichtbögen ingefolge eigenmagnetischer Kompression. *Z. Physik* 141:198-216.

24. Woods, R. A., and Milner, D. R. 1971. Motion in the weld pool in arc welding. *Welding Journal* 50(4):163-s to 173-s.

25. Tritton, D. J. 1977. *Physical Fluid Dynamics.* New York: Van Nostrand.

26. Keene, B. J., Mills, K. C., Bryant, J. W., and Hondros, E. D. 1982. Effects of interaction between surface active elements on the surface tension of iron. *Canadian Metallurgical Quarterly* 21(4):393-403.

27. Heiple, C. R., and Roper, J. R. 1982. Mechanism for minor element effect on GTA fusion zone geometry. *Welding Journal*

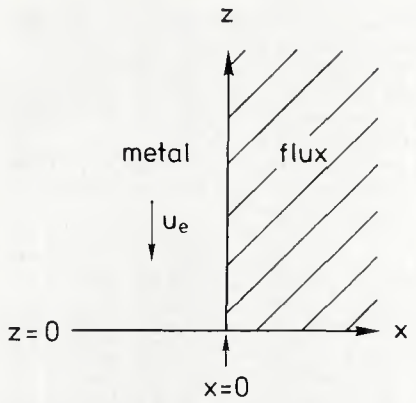

Fig. 16—Heat flow from core into covering

61(4):97-s to 102-s.

28. Roberts, P. H. 1967. *An introduction to magnetohydrodynamics.* London: Longmans.

29. Wilson, J. L., Claussen, G. E., and Jackson, C. E. 1956. The effect of I^2R heating on electrode melting rate. *Welding Journal* 35(1):1-s to 8-s.

30. Halmøy, E. 1979. Wire melting rate, droplet temperature and effective anode melting potential. *Proc. Int. Conf. on Arc Physics and Weld Pool Behaviour, London,* pp. 49-57. Abington, Cambridge: The Welding Institute.

31. Hummitzsch, W., and Zollenkopf, H. 1964. Die elektrische Leitfähigkeit der Umhüllungen und Schlacken von Schweisselektroden. *Schweissen und Schneiden* 16(2):45-50.

32. Grigull, U., and Sandner, H. 1979. *Wärmeleitung.* Berlin: Springer.

33. Ton, H. 1975. Physical properties of the plasma-MIG welding arc. *J. Phys. D* 8:922-933.

Appendix

A. Determination of Thermal Properties

It follows from the relations given in Ref. 10, Sec. 2.15, that the heat current density, q, at the boundary, at $t > t_0$, is given by:

$$q = \frac{T_1 - T_0}{\{(\lambda_w \rho_w c_{pw})^{-1/2} + (\lambda_f \rho_f c_{pf})^{-1/2}\}\{\pi (t - t_0)^{1/2}} \quad (A1)$$

The heat content of the wire decreases according to:

$$\frac{dH}{dt} = -\frac{4q}{d_w \rho_w} \quad (A2)$$

Equations (A1) and (A2) give equation (2).

B. Calculation of Heat Flow into Coating in Transition Region behind Melting Front

The geometry is taken as in Fig. 16. The material is moving into the negative z-direction at a velocity u_e; the melting front remains at z = 0. Both for metal and flux we have:

$$u_e \frac{\partial T}{\partial z} + a\nabla^2 T = 0 \quad (B1)$$

with $a = a_w$ for the metal, and $a = a_f$ for the coating.

The temperature in the metal core, T_c, is practically independent of the radial coordinate because of the high thermal conductivity, and T_c is taken to be a function of z only. It then follows that:

$$\lambda_w S_w T_c'' + u_e S_w \rho_w c_{pw} T_c' - \pi d_w q = 0 \quad (B2)$$

where q is the heat current density into the positive x-direction at x = 0, and the differentiation is with respect to z. Boundary conditions are that $T_c = T_{mp}$ for z = 0, and $T_c \to T_w$ for $z \to \infty$.

For q = 0 it follows that:

$$T_c = T_w + \Delta T \exp(-p z) \quad (B3)$$

with $p = p_0 = u_e/a_w$, and $\Delta T = T_{mp} - T_w$.

It is now assumed that the depth of penetration of the heat into the covering is small with respect to the radius of the core and the thickness of the coating, *i.e.*, it is assumed that the boundary between metal and flux is a plane and that the coating is infinitely thick. Furthermore, we take T_c to be given by equation (B3), with p still to be determined. The temperature of the flux T, is then given by

$$u_e \frac{\partial T}{\partial z} + a_f \left(\frac{\partial^2 T}{\partial x^2} + \frac{\partial^2 T}{\partial z^2}\right) = 0 \quad (B4)$$

with boundary conditions that $T(x = 0,z) = T_c(z)$, $T \to T_w$ for $z \to \infty$, and $T \to T_w$ for $x \to \infty$. A solution to equation (B4) is:

$$T = T_{mp} + \Delta T \exp(-p z) \exp(-r x)$$

where p and r are constants. Using $a_w \gg a_f$ and neglecting higher order terms, we obtain $p \approx p_0$, and $r \approx u_e/(a_w a_f)^{1/2}$. Since

$q = -\lambda_f (\partial T/\partial x)_{x=0}$; it follows that:

$$q \approx \frac{\lambda_f u_e \Delta T}{(a_w a_f)^{1/2}} \exp(-p_0 z) \quad (B5)$$

The thermal power transferred from the metal to the flux in cylindrical geometry is:

$$\Phi_f = \pi d_w \int_0^\infty q \, dz.$$

Taking q as found for plane geometry (equation (B5)) we obtain

$$\Phi_f \approx \pi d_w \lambda_f (a_w/a_f)^{1/2} \Delta T \quad (B6)$$

The difference ΔT was taken as $\Delta T = T_{mp} - T_0$, *i.e.*, the increase in T_w due to Joule heating was neglected.

The assumptions of plane geometry and infinite coating thickness are justified if the heat does not penetrate deeply into the covering, *i.e.*, if $\exp(-r \Delta x) < \delta$, where Δx is the thickness of the coating, and δ some small number. Taking $\delta = 0.1$, we find as the condition for the applicability of equation (B6) that $u_e \cdot \Delta x > (a_w/a_f)^{1/2} |\ln 0.1|$. Some of the experiments yielded values of $u_e \cdot \Delta x$ below this limit. The approximation to be given below was used when $u_e \cdot \Delta x > (a_w/a_f)^{1/2} |\ln 0.2|$, and the average of the two approximations was used in intermediate cases.

If the heat does penetrate right through the coating, then it is appropriate to introduce an average flux temperature $\bar{T}_f$, this average being taken over a cross-section perpendicular to the cylinder axis. The temperature distribution is again stationary ($\partial/\partial t = 0$) and it follows that:

$$\pi d_w q + u_e S_f \rho_f c_{pf} \bar{T}_f' = 0 \quad (B7)$$

where S_f is the cross-sectional area of the covering, and the differentiation is with respect to z. Equation (B2) is retained, and for q we write:

$$q = 2\lambda_f (T_c - \bar{T}_f)/\Delta x \quad (B8)$$

Boundary conditions are that $T_c = T_m$ at z = 0, and that T_c and T_f go to T_w at large z. It now follows in a straightforward manner that the solution for T_c is given by equation (B3), where p is the positive root of the equation

$$p^2 + p p_0 (A - 1) - A p_0^2 (B + 1) = 0$$

where $A = 2\pi d_w a_w a_f/(\Delta x S_f u_e^2)$

and $B = S_w \rho_w c_{pw}/(S_f \rho_f c_{pf})$

It also follows that:

$$\Phi_f = \lambda_w S_w \Delta T(p - p_0) \quad (B9)$$